Nonlinear Processes in Geophysics (2002) 9: 311–323

Nonlinear Processes in Geophysics


# Controlling thermal chaos in the mantle by positive feedback from radiative thermal conductivity

**F. Dubuffet, D. A. Yuen, and E. S. G. Rainey**

Minnesota Supercomputing Institute and Dept. of Geology and Geophysics, University of Minnesota, Minneapolis, MN 55415-1227, USA

Received: 17 July 2001 – Accepted: 22 October 2001

**Abstract.** The thermal conductivity of mantle materials has two components, the lattice component $k_{lat}$ from phonons and the radiative component $k_{rad}$ due to photons. These two contributions of variable thermal conductivity have a nonlinear dependence in the temperature, thus endowing the temperature equation in mantle convection with a strongly nonlinear character. The temperature derivatives of these two mechanisms have different signs, with $\partial k_{lat}/\partial T$ negative and $dk_{rad}/dT$ positive. This offers the possibility for the radiative conductivity to control the chaotic boundary layer instabilities developed in the deep mantle. We have parameterized the weight factor between $k_{rad}$ and $k_{lat}$ with a dimensionless parameter $f$, where $f = 1$ corresponds to the reference conductivity model. We have carried out two-dimensional, time-dependent calculations for variable thermal conductivity but constant viscosity in an aspect-ratio 6 box for surface Rayleigh numbers between $10^6$ and $5 \times 10^6$. The averaged Péclet $\langle Pe \rangle$ numbers of these flows lie between 200 and 2000. Along the boundary in $f$ separating the chaotic and steady-state solutions, the $\langle Pe \rangle$ number decreases and the Nusselt number increases with internal heating, illustrating the feedback between internal heating and radiative thermal conductivity. For purely basal heating situation, the time-dependent chaotic flows become stabilized for values of $f$ of between 1.5 and 2. The bottom thermal boundary layer thickens and the surface heat flow increases with larger amounts of radiative conductivity. For magnitudes of internal heating characteristic of a chondritic mantle, much larger values of $f$, exceeding 10, are required to quench the bottom boundary layer instabilities. By isolating the individual conductive mechanisms, we have ascertained that the lattice conductivity is partly responsible for inducing boundary layer instabilities, while the radiative conductivity and purely depth-dependent conductivity exert a stabilizing influence and help to control thermal chaos developed in the deep mantle. These results have been verified to exist also in three-dimensional geometry and would argue for the need to consider the potentially important role played by radiative thermal conductivity in controlling chaotic flows in time-dependent mantle convection, the mantle heat transfer, the number of hotspots and the attendant mixing of geochemical anomalies.

*Correspondence to:* F. Dubuffet (fabien@msi.umn.edu)

## 1 Introduction

Both the transport properties of momentum and heat in the Earth's mantle are dependent on both the temperature and depth. On the one side, in the past thirty years, since the advent of plate tectonics much attention has been paid to the temperature-dependence of mantle viscosity because of the feedback on the thermal evolution of the mantle (Tozer, 1965, 1972), and the influence of the strong lithosphere on the style of planetary convection (Richter et al., 1983; Ogawa et al., 1991; Solomatov and Moresi, 2000; Monnereau and Quéré, 2001) and the development of fast narrow plumes (Yuen et al., 1976; Christensen, 1984; Olson et al., 1988; Larsen and Yuen, 1997; Thompson and Tackley, 1998). On the other side, not much attention has been devoted to thermal conductivity.

It is well known from solid-state physics that heat is transported by conduction in crystalline solids by means of both phonon and photon propagation (e.g. Ziman, 1962). Recently a semi-empirical theory for mantle thermal conductivity based on absorption and reflection spectroscopy has been worked out by Hofmeister (1999, 2001). This conductivity model $k(T, z)$, which depends on the temperature $(T)$ and depth $(z)$, has contributions from both the phonon and photon transport mechanisms and has a nonlinear dependence in the temperature. The temperature equation contains now three nonlinear terms (e.g. Dubuffet et al., 1999), thus replacing the simple Laplacian terms for linear heat diffusion as in the case for constant thermal conductivity. The dynamical effects of these conductivity nonlinearities in mantle convection are manifold, such as a more focussed plume (Dubuffet and Yuen, 2000) and a hotter interior (Dubuffet et al., 1999). Because of these nonlinearities, the temperature equa-

tion changes from a simple advection-diffusion equation to a more complicated nonlinear advection-diffusion equation with a mixed parabolic and hyperbolic character, similar to the Kardar-Parisi-Zhang equation for growing interface (Kardar et al., 1986) and used in geomorphology (Pelletier, 1999).

An outstanding characteristic concerning the temperature-dependence of thermal conductivity is the distinct difference between the temperature-dependence of the lattice conductivity $k_{lat}(T, z)$ and that of the radiative conductivity $k_{rad}(T)$ from the photons. The temperature-dependence of $k_{lat}(T, z)$ behaves similarly to the viscosity in that $\partial k_{lat}/\partial T$ is negative, while from local radiative equilibrium (e.g. Siegel and Howell, 1972) it is well known that $dk_{rad}(T)/dT$ is positive. Such a sign difference in the temperature derivatives of the two components of the conductivity would mean that the two mechanisms would work against each other in matters concerning the boundary layer stability in mantle convection.

From a simple physical argument, one would expect $k_{rad}$ to be stabilizing, since an increase in temperature would increase $k_{rad}$, which would decrease the local Rayleigh number and also broaden the wavelength of the thermal disturbance, thus suppressing small-scale boundary layer instabilities. This stabilizing phenomenon has already been observed in the finite amplitude convection calculations by Matyska et al. (1994) in which only $k_{rad}(T)$ was employed for the conductivity. Since the distribution of the relative proportions between $k_{lat}$ and $k_{rad}$ is still a subject of debate (Shankland et al., 1979) and also of active study (Hofmeister, 1999; Hofmeister, 2001), we will investigate the role played by $k_{rad}$ in stabilizing time-dependent convection. We will employ a simple parameter, called $f$, which measures the relative importance between $k_{rad}$ and $k_{lat}$ and then vary this parameter to study the possibility for controlling thermal chaotic motions in mantle convection by increasing the value of this parameter. This type of approach is very much akin to the spirit of controlling spatial-temporal chaos, which today is one of the central problems in nonlinear dynamics (e.g. Ott et al., 1994; Kim et al., 2001).

In Sect. 2 we will describe the thermal conductivity model, the scheme of parameterizing the relative importance of $k_{rad}$ to $k_{lat}$, and the numerical model for thermal convection with variable thermal conductivity. In Sect. 3 we will focus primarily on the 2-D results in which the time-dependence in mantle convection is shown to be controllable by the growing influence of radiative thermal conductivity. We will also corroborate with 3-D calculations. In the final section we discuss the results and the geophysical implications of this new physical mechanism for stabilizing boundary layer instabilities and influencing global geodynamics.

## 2 Description of the thermal conductivity and numerical model

First, we describe the thermal mantle conductivity model, which comes from Hofmeister (1999, 2001). It has both the $k_{lat}(T, z)$ and $k_{rad}(T)$. There is a parameter "$a$" in $k_{lat}(T, z)$ (Eq. 2) which can account for the type of chemical bonding in mantle minerals (Hofmeister, 1999). These expressions, based on experimental phonon lifetimes and reflectance data, take the form:

$$k_{rad}(T) = \sum_{i=0}^{3} b_i T^i \tag{1}$$

where the radiative portion has contributions from $T$ and $T^2$ as well as $T^3$, because of the use of the overtone modes (Hofmeister, 1999).

$$k_{lat}(T, z) = k_0 \left(\frac{298}{T}\right)^a \exp\left(\left(-4\gamma + \frac{1}{3}\right)\int_{298}^{T} \alpha(\theta) d\theta\right)\left(1 + \rho g \frac{K' z}{K}\right) \tag{2}$$

We note that $k_{lat}(T, z)$ has two nonlinear dependences with $T$, one exponential and the other power-law. The names and parameter values associated with thermal conductivity are provided in Table 1.

As discussed above, $k_{lat}$ behaves like mantle viscosity in that it decreases with a hotter temperature and increases with greater pressure. However, $k_{rad}$ acts in the opposite fashion, it increases with higher temperature. Because of the rapid rise in the temperature within the boundary layer, $k_{rad}$ would increase a lot locally, while $k_{lat}$ would decrease much locally. In order to study the influence of an enhanced radiative contribution to the total thermal conductivity, we have simply multiplied the radiative thermal conductivity by a weight factor $f$. This weight factor $f$ will be regarded in this stability study as a control variable. Thus the expression of the thermal conductivity used in this study is:

$$k(T, z) = f \times k_{rad}(T) + k_{lat}(T, z) \tag{3}$$

We will vary $f$ in Eq. 3 and study its influence on the stability of the global convective dynamics. Let us emphasize here that $f$ is not to be regarded as having any strict physical interpretation in terms of solid-state physics but rather as a control variable for quantifying the character of the flow. Van den Berg et al. (2002) have used this type of weight factoring in $f$ to study the effects of varying $f$ on the thermal evolution of the mantle.

We have studied this problem of the influence of radiative conductivity with a simple constant viscosity convection model in the Boussinesq limit but with variable thermal conductivity. The equations of convection for an infinite Prandtl number fluid are solved in a 2-D Cartesian geometry. The coordinates are $x$ and $z$, with $z$ the vertical axis pointing downwards. With a variable thermal conductivity, the dimensionless temperature equation takes the following form:

$$\frac{DT}{Dt} = \kappa(T, z)\nabla^2 T + \frac{\partial \kappa}{\partial T}(T, z)\,(\nabla T)^2 + \frac{\partial \kappa}{\partial z}(T, z)\frac{\partial T}{\partial z} + R \tag{4}$$

**Table 1.** Values of the conductivity parameters (from Hofmeister, 1999)

| Parameter | Definition | Value | unit |
|---|---|---|---|
| $b_0$ | Constant associated with radiation | $1.753 \times 10^{-2}$ | $W.m^{-1}.K^{-1}$ |
| $b_1$ | " | $-1.0365 \times 10^{-4}$ | $W.m^{-1}.K^{-2}$ |
| $b_2$ | " | $2.2451 \times 10^{-7}$ | $W.m^{-1}.K^{-3}$ |
| $b_3$ | " | $-3.407 \times 10^{-11}$ | $W.m^{-1}.K^{-4}$ |
| $a$ | Power-law index | 0.9 | |
| $\kappa_0$ | Surface thermal diffusivity | $0.91 \times 10^{-6}$ | $m^2.s^{-1}$ |
| $\gamma$ | Grüneisen parameter | 1.2 | |
| $K$ | Bulk modulus | 265 | GPa |
| $K'$ | Pressure derivative of the bulk modulus | 5 | |

**Table 2.** Values of the parameters used in the thermal convection model

| Parameter | Definition | Value | unit |
|---|---|---|---|
| $h$ | Mantle thickness | $2.88 \times 10^6$ | m |
| $\Delta T$ | Temperature difference across the mantle | 2702 | K |
| $\alpha$ | Thermal expansivity | $2 \times 10^{-5}$ | $K^{-1}$ |
| $H$ | Chondritic abundance of heating | $6 \times 10^{-12}$ | $W.Kg^{-1}$ |
| $k_0$ | Surface thermal conductivity | 3.3 | $W.K^{-1}.m^{-1}$ |
| $g$ | Gravity | 9.81 | $m.s^{-2}$ |

where $D/Dt$ is the substantive derivative and $\kappa(T,z) = k(T,z)/\left(\rho C_p \kappa_0\right)$ is the dimensionless thermal diffusivity. We refer the reader to Table 2 for the definitions and parameter values. The dimensionless internal heating parameter $R$ is given by:

$$R = \frac{Hd^2}{k_0 \Delta T} \tag{5}$$

$k_0$ is given in Table 2. A typical value for radioactive internal heating $R$ is around 12 based on the chondritic abundance from meteorites (Leitch and Yuen 1989). We will study the effects of varying $f$ in stabilizing flows for different amounts of $R$, varying from $R = 0$ (purely base-heated configuration) to the chondritic value. The particular temperature at the base of the mantle plays an important role in the radiative heat transfer. We note that the temperature of 3000 K assumed at the core-mantle boundary is on the low side (Zerr et al., 1998).

We note that the three terms on the right hand side of the temperature equation are non-linear because of the variable thermal conductivity, instead of the linear diffusion term in the constant conductivity case. An alternating-direction-implicit (ADI) scheme (e.g. Morton and Mayers, 1994) and the finite difference method are used to solve the temperature (Eq. 4). This implicit scheme is of second order of accuracy in space and time. The constant viscosity momentum (Eq. 6), which is unaffected by the introduction of variable conductivity, is solved in the spectral domain, using a Fast Fourier Transform along the horizontal and a second-order

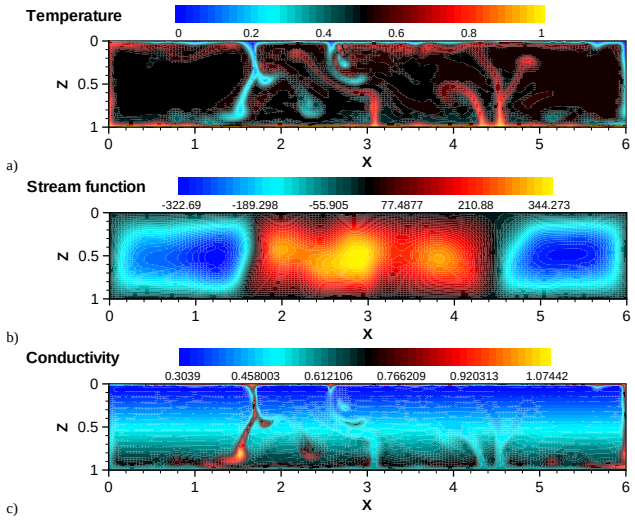


**Fig. 1.** Temperature field **(a)**, stream function **(b)**, and thermal conductivity field **(c)**, for a model with a Rayleigh number of $Ra = 10^6$, a dimensionless internal heating rate of $R = 0$, and a weight factor $f = 1.0$. $1025 \times 512$ grid points are used in a box with an aspect ratio 6.

finite-difference scheme in the vertical directionfor each horizontal wave number.

$$\nabla^4 \phi = -Ra_s \frac{\partial T}{\partial x} \tag{6}$$

$\phi$ is the stream function, the other parameters are defined in Table 2, where $Ra_s$ is the surface Rayleigh number.

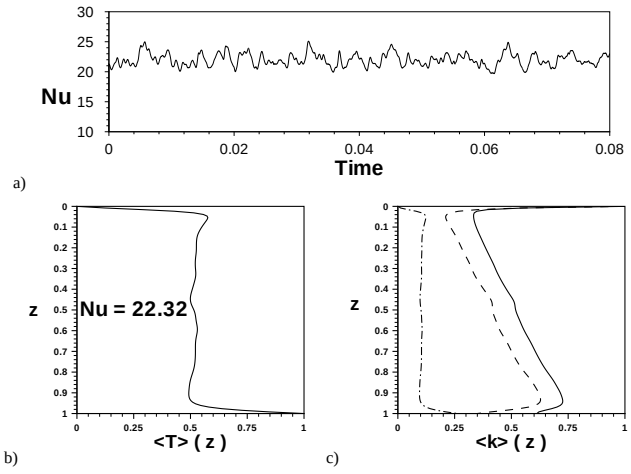


**Fig. 2.** Evolution with time of the surface Nusselt number **(a)**, horizontally averaged temperature profile $\langle T(z)\rangle$ **(b)**, and the horizontally averaged conductivity profiles $\langle k_{rad}\rangle$ (dashed-dotted line), $\langle k_{lat}\rangle$ (dashed line) and $\langle k\rangle$ (solid line) **(c)**, for a model with a Rayleigh number of $Ra = 10^6$, a dimensionless internal heating rate of $R = 0$, and a weight factor $f = 1.0$. For simplicity, the surface Nusselt number is defined as $Nu = \langle \partial T/\partial z\rangle$
. The brackets denote horizontal average.

The thermal and free-slip boundary conditions are imposed at the top and bottom boundaries, where the temperatures are specified, and the horizontal boundaries are impermeable. We note that the particular value of the temperature assumed at the bottom boundary or the core-mantle boundary (CMB) will exert a definite dynamical influence, because of the intrinsic temperature-dependent nonlinearity in the thermal conductivity. In order to resolve correctly the temperature and thermal conductivity gradients in the boundary layers, more grid points are necessary in the numerical experiments involving variable thermal conductivity than in the constant conductivity cases (Dubuffet et al., 1999). We have used a grid consisting of $1025 \times 257$ points in a box of aspect ratio 6 for all models presented in this study.

## 3 Results

The values of the parameter "$a$" in the lattice conductivity, the bulk modulus $K$, and the derivative of the bulk modulus $K'$, in $k_{lat}$, are all functions of the composition of mantle rocks. We have chosen values (see Table 1) suitable for the lower mantle (Hofmeister, 1999). In Figs. 1 to 8, we present the temperature, stream function conductivity fields, the horizontally averaged temperature and thermal conductivity profiles for different values of the parameter $f$, different dimensionless heating rate $R$ but for the same Rayleigh number of $10^6$. Figure 1 displays the results for the case $f = 1$ and $R = 0$. The temperature field (Fig. 1a) shows clearly an unsteady flow with thermal boundary layers instabilities in the top and bottom boundary layers. Plume branching ($x = 4.6$), resulting from the growth of secondary instabilities in the plume, appears at this Rayleigh number. Such kind of plume branching is present in convective flows with constant thermal conductivity at higher Rayleigh number, $Ra$ greater than $10^9$ (Vincent and Yuen, 2000). This type of behaviour has already been observed in convection modeling with a non-Newtonian viscosity for effective Rayleigh numbers of the same order of magnitude (Malevsky et al., 1992). The enhancement of plume branching at lower Rayleigh number comes from the non-linearities introduced by the variable viscosity in the momentum equation (Malevsky et al., 1992) and here by the variable thermal conductivity in the energy equation. Three cells (Fig. 1b) are present in this model. Even though the flow is unsteady due to boundary layer instabilities, a large scale flow exists (Hansen and Ebel, 1988). The conductivity field (Fig. 1c) shows a strong decrease of the conductivity in the top thermal boundary layer due to the strong increase of the temperature, leading to a decrease of the lattice thermal conductivity ($k_{lat}$). The conductivity slightly increases with depth due to the hydrostatic pressure effects in $k_{lat}(T, z)$. The conductivity is greater than the ambient value in downwellings and smaller in the plumes located near the bottom boundary layer. The smaller conductivity inside the plumes traps the heat inside. After being trapped, the hot anomaly is released close to the surface, thus creating a hot and thin layer beneath the top boundary layer (Fig. 1a). A low conductivity layer is associated with this hot layer under the surface. The conductivity field clearly shows that the variations of the thermal conductivity are essentially due to the variations of $k_{lat}$. In a previous study (Dubuffet et al., 1999), we have shown that for $f = 1$, $k_{rad}$ is smaller than $k_{lat}$ in an horizontally averaged sense. In Fig. 2 we show the evolution of the surface Nusselt number with time (Fig. 2a), the horizontally averaged temperature profile $\langle T\rangle$ and the horizontally averaged conductivity $\langle k\rangle$ with the radiative component $\langle k_{rad}\rangle$ (dashed-dotted line) and the lattice component $\langle k_{lat}\rangle$ (dashed line). The Nusselt number is defined here to be $\langle \partial T/\partial z\rangle$, the horizontally averaged value of the vertical temperature gradient, as we have not solved the nonlinear two-point boundary value problem for the background temperature in the presence of variable thermal conductivity. We note that the $\langle k_{rad}\rangle$ mimicks the $\langle T\rangle$ profile and increases at the bottom, while both the $\langle k_{lat}\rangle$ and $\langle k\rangle$ develop a low conductivity zones at the base of the top boundary layer and at the bottom. In spite of the pressure-dependence of conductivity the value of $\langle k\rangle$ in the lower mantle is smaller than the surface value because of the strong decrease of the thermal conductivity with depth from $k_{lat}(T)$.

Now we have increased the value $f$ gradually from 1 to 1.2 and so on in an incremental manner. In Fig. 3, we display the results for the same values of parameters as in Fig. 1 ($Ra = 10^6$ and $R = 0$) but now, we have multiplied the radiative component ($k_{rad}$) by a factor $f = 1.5$. The flow shows a more quiescent behaviour (Fig. 3a). Thermal boundary layer instabilities are found only in the bottom boundary layer. As in the previous case (Fig. 1), we note the presence of a hot thermal layer under the top cold boundary layer (Dubuffet et al., 2000b). Increasing the parameter $f$ from 1

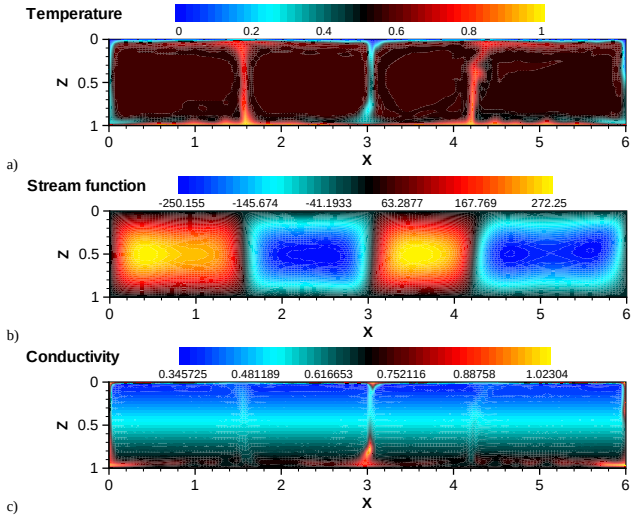


**Fig. 3.** Temperature field **(a)**, stream function **(b)**, and thermal conductivity field **(c)**, for a model with a Rayleigh number of $Ra = 10^6$, a dimensionless internal heating rate of $R = 0$, and a weight factor $f = 1.5$.

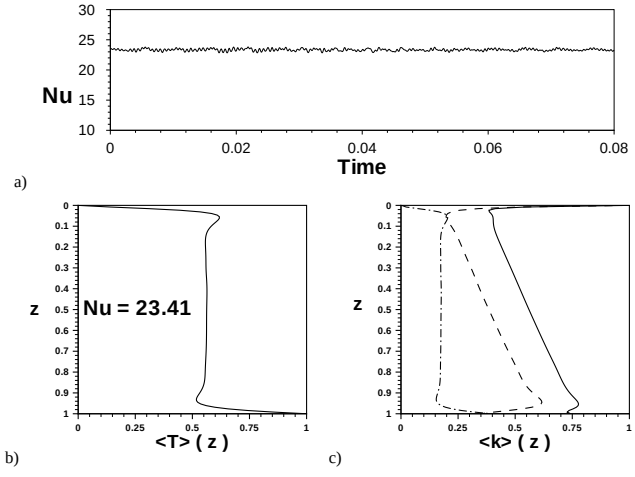


**Fig. 4.** Evolution with time of the surface Nusselt number **(a)**, horizontally temperature profile $\langle T \rangle(z)$ **(b)**, and the horizontally averaged conductivity profiles $\langle k_{rad} \rangle$ (dashed-dotted line), $\langle k_{lat} \rangle$ (dashed line) and $\langle k \rangle$ (solid line) **(c)**, for a model with a Rayleigh number of $Ra = 10^6$, a dimensionless internal heating rate of $R = 0$, and a weight factor $f = 1.5$.

(Fig. 1b) to 1.5 (Fig. 3b) leads to a slight increase the numbers of cells. The convective flow is now composed of 4 cells, with 2 cells that have the same size 1.5 (located between $x = 0$ and $x = 3$) . Thus the number of upwellings is changed by an enhanced radiative conductivity. We note that the size of the cells is more similar than in the case $f = 1$ (Fig. 1b). The conductivity (Fig. 3c) decreases in the top boundary layer. This conductivity is smaller than the surrounding one, in the downwelling flows. But now the value of the conductivity in the center of downwellings located in the center of the box ($z = 0.5$) is around $2.2\,\mathrm{W.K^{-1}.m^{-1}}$,

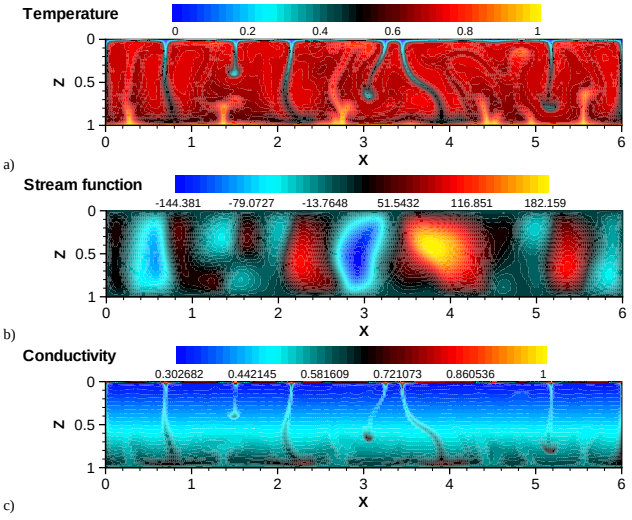


**Fig. 5.** Temperature field **(a)**, stream function **(b)**, and the conductivity field **(c)**, for a model with a Rayleigh number of $Ra = 10^6$, a dimensionless internal heating rate of $R = 5$, and a weight factor $f = 1$.

whereas the value was around $2.6\,\mathrm{W.K^{-1}.m^{-1}}$ in the case $f = 1$ (Fig. 1c). Although these changes in the conductivity are small, they do exert a great deal of influence on the boundary layer stability. In the center of the plumes, in the lower part of the box (see $z = 0.6$), the conductivity is slightly higher (around $2\,\mathrm{W.K^{-1}.m^{-1}}$) than the conductivity in the plume near the center (around $1.9\,\mathrm{W.K^{-1}.m^{-1}}$). At this depth ($z = 0.6$), the surrounding flow, has a conductivity of around $2\,\mathrm{W.K^{-1}.m^{-1}}$. At a shallower depth, the conductivity becomes more uniform inside the plume and is higher than the surrounding (see $z = 0.2$). In the lower mantle, there exists a high conductivity layer due to the increase in $k_{rad}(T)$. The value of $f = 1.5$ appears to be a critical value above which the flow is steady. The resolution of $f_c$ for this $Ra$ is 0.5, i.e. solutions at $f = 2.0$ appear quite similar to $f = 1.5$. Further increase in $f$ to $f = 3.0$ would bring about a steady state. From now on, we will designate the critical value of $f$ for this transition to be $f_c$. In Fig. 4 we plot the associated Nusselt number evolution, $\langle T \rangle$, $\langle k_{rad} \rangle$, $\langle k_{lat} \rangle$ and $\langle k \rangle$. The Nusselt number and $\langle k_{rad} \rangle$ both increase with $f$.

As is well known, internal heating causes a greater time-dependence in mantle convection (McKenzie et al., 1974). Therefore, we have put in a moderate amount of internal-heating $R = 5$, around half the chondritic value in order to determine the critical value of $f$ required for stabilizing flows with only a small amount of radioactive heating. We show in the next four figures (Fig. 5 to Fig. 8) the results of the numerical modeling, for two cases with $R = 5$ and a Rayleigh number of $Ra = 10^6$. The parameter $f$ is set to 1 in Fig. 5. The flow produces a chaotic behaviour (Fig. 5a) more so than with $R = 0$ and $f = 1$. There are more upwellings and downwelling than in the pure-basal heating case ($R = 0$) (Fig. 1a). Both internal heating and variable thermal conductivity drive a greater asymmetry between the top

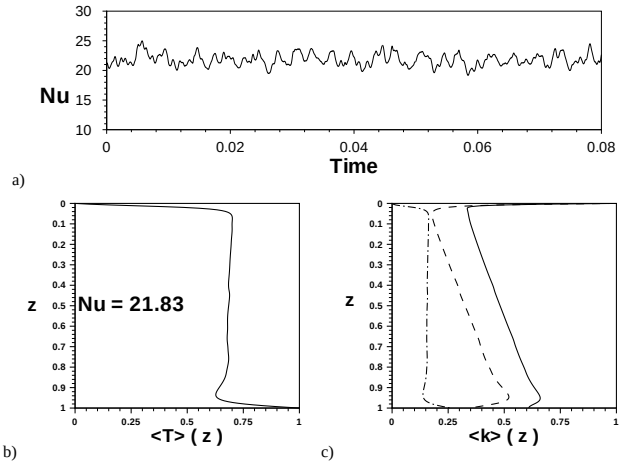


**Fig. 6.** Evolution with time of the surface Nusselt number **(a)**, horizontally averaged temperature $\langle T \rangle(z)$ **(b)**, and the horizontally averaged conductivity profiles $\langle k_{rad} \rangle$ (dashed-dotted line), $\langle k_{lat} \rangle$ (dashed line) and $\langle k \rangle$ (solid line) **(c)**, for a model with a Rayleigh number of $Ra = 10^6$, a dimensionless internal heating rate of $R = 5$, and a weight factor $f = 1$.

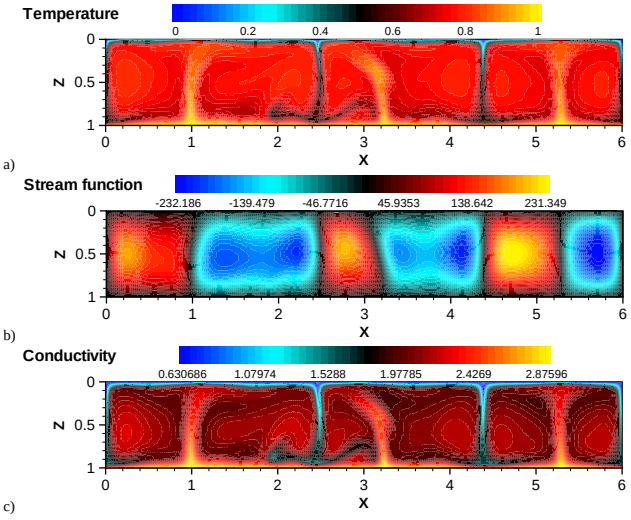


**Fig. 7.** Temperature field **(a)**, stream function **(b)**, and conductivity field **(c)**, for a model with a Rayleigh number of $Ra = 10^6$, a dimensionless internal heating rate of $R = 5$, and a weight factor $f = 8$.

and bottom boundary layers. The downwelling currents are stronger than the upwelling plumes. The flow with internal heating consists of 12 cells (Fig. 5b), much more numerous than the purely basal-heating case (Fig. 1b). The conductivity field (Fig. 5c) shows the same behaviour than in the case with $R = 0$ and $f = 1$. This results in a strong decrease of the conductivity in the upper boundary layer, a smaller conductivity than the surrounding in the plumes, a higher conductivity in the downwellings, a low conductivity layer under the top thermal boundary layer and an increase in the conductivity with depth outside the boundary layers. These changes represent then the characteristic properties of the variable thermal conductivity with $f = 1$. But with internal heating, the value of the conductivity is smaller in the downwellings (around $1.6\,\mathrm{W.K^{-1}.m^{-1}}$) than in the case without heating ($R = 0$). The conductivity is now slightly higher at the base of the plumes (at $z = 0.8$) than in the downwellings. These new effects are caused by the higher interior temperature induced by the internal heating. The increase of the interior temperature leads to a decrease in the lattice component of the conductivity ($k_{lat}$), and an increase in the radiative component ($k_{rad}$). Figure 6 displays the associated Nusselt number evolution, $\langle T \rangle$, $\langle k_{lat} \rangle$, $\langle k_{rad} \rangle$ and $\langle k \rangle$ profiles. Internal heating decreases the trough in the conductivity near the CMB.

In order to determine the critical value of $f$, above which we can stabilize the flow with an dimensionless internal heating rate of $R = 5$, we have carried out numerical simulations at incremental steps of $f$ up to 12. In Fig. 7, we show the results for a value of $f = 8$ and $R = 5$. The temperature field (Fig. 7a) and the stream function (Fig. 7b) reveal a much more stable flow with fewer upwellings than in the case with $f = 1$ (Fig. 5). It consists of 3 plumes and 4 downwellings. The number of convective cells is 6. By increasing the weight factor $f$ to 8, we observe a decrease in the number of cells. The conductivity field (Fig. 7c) shows much larger variations of the conductivity, between $2\,\mathrm{W.K^{-1}.m^{-1}}$ and $9\,\mathrm{W.K^{-1}.m^{-1}}$, than in the case with $f = 1$ where the conductivity varies between $1\,\mathrm{W.K^{-1}.m^{-1}}$ and $3.2\,\mathrm{W.K^{-1}.m^{-1}}$. In the model with $R = 5$ and $f = 8$ (Fig. 7c), the conductivity increases in both thermal boundary layers whereas in the model with $R = 5$ and $f = 1$ (Fig. 5c), the conductivity decreases in the upper thermal boundary layer and it becomes nearly constant in the bottom boundary layer. This results in

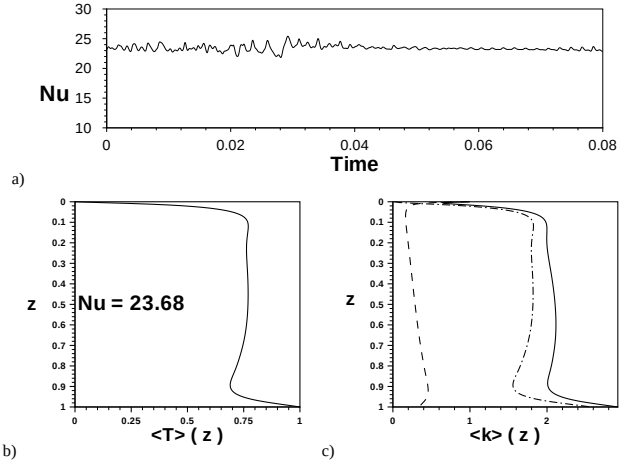


**Fig. 8.** Evolution with time of the surface Nusselt number **(a)**, horizontally averaged temperature profile $\langle T \rangle(z)$ **(b)**, and the horizontally averaged conductivity profiles $\langle k_{rad} \rangle$ (dashed-dotted line), $\langle k_{lat} \rangle$ (dashed line) and $\langle k \rangle$ (solid line) **(c)**, for a model with a Rayleigh number of $Ra = 10^6$, a dimensionless internal heating rate of $R = 5$, and a weight factor $f = 8$.

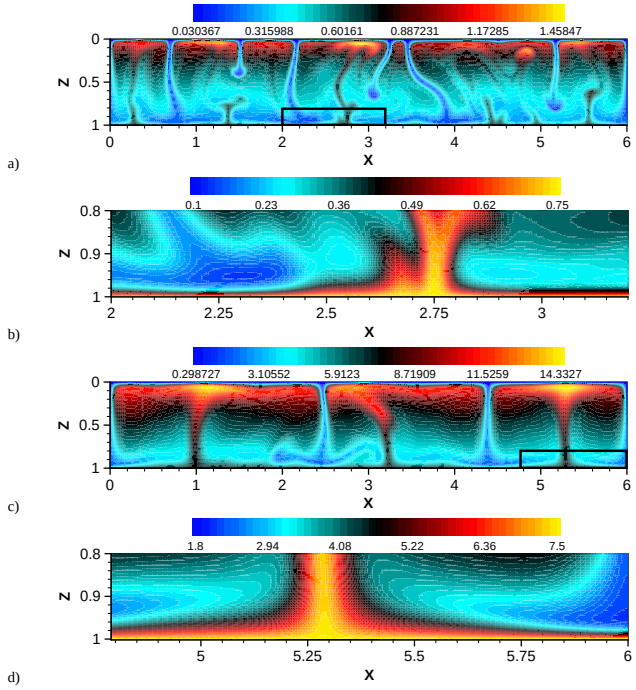


**Fig. 9.** Maps showing the ratio between the radiative thermal conductivity $k_{rad}$ and the lattice component $k_{lat}$. **(a)** and **(b)** show this ratio for the model with $R = 5$ and $f = 1$ (Fig. 5), **(c)** and **(d)** for the model with $R = 5$ and $f = 8$ (Fig. 7). We show this ratio in the small boxes located at the bottom fifth of the box in the panels (a) and (c) in panels (b) and (d), respectively.

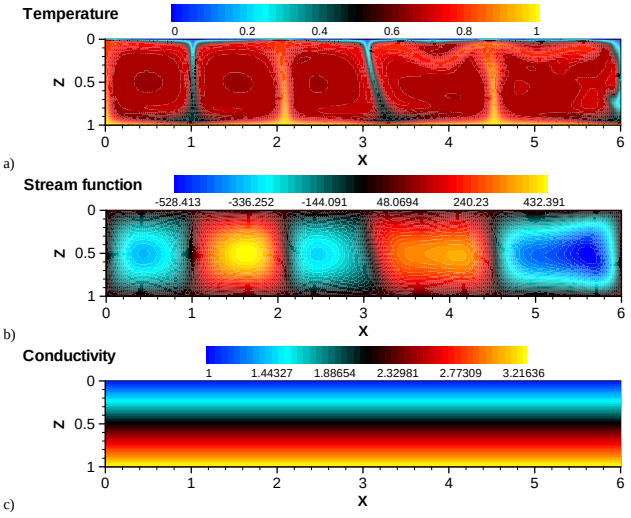


**Fig. 10.** Temperature field **(a)**, stream function **(b)**, and thermal conductivity field **(c)**, for the model with the expression for thermal conductivity $k(z) = k_{lat}(z)$ (Eq. 7), $Ra = 10^6$ and $R = 0$.

a decrease of the local Rayleigh number in the boundary layers associated with the model having $R = 5$ and $f = 8$, thus leading to a general degree of stabilization of the global flow. These variations of the thermal conductivity in the boundary layers are caused by the variations of the radiative component $k_{rad}(T)$. We have found that $f = 8$ is around the characteristic value of above which the flow becomes quasi-steady. We can thus claim for $R = 5$ that the critical value $f_c$ is around 8. Figure 8 shows the associated Nusselt number evolution, the $\langle T \rangle$, $\langle k_{lat} \rangle$, $\langle k_{rad} \rangle$ and the $\langle k \rangle$ profiles. Because of the high interior temperature, $\langle k_{rad} \rangle$ now becomes much larger than $\langle k_{lat} \rangle$. Thus the $\langle k \rangle$ profile resembles the $\langle T \rangle$ profile. This change in the $\langle k \rangle$ profile with increasing $f$ is responsible for the stabilization of the plumes.

We will now demonstrate that an increase in the local radiative thermal conductivity ($k_{rad}(T)$) versus the lattice conductivity $k_{lat}(T, z)$ would lead to a stabilization of the global flow, as shown previously in Fig. 8. This phenomenon is illustrated in Fig. 9, which shows a 2-D map showing the ratio of $k_{rad}/k_{lat}$ for the model with $R = 5$ and $f = 1$ (Fig. 9a and b), and for the more radiatively pacified model with $R = 5$ and $f = 8$ (Fig. 9c and d). The model with $R = 5$ and $f = 1$ has a radiative conductivity smaller than the lattice conductivity in the thermal boundary layers, in the downwellings and in the plumes at the bottom. The ratio $k_{rad}/k_{lat}$ is smaller in the downwellings than in the plumes because of a high radiative conductivity and a small lattice conductivity resulting from the high temperature in the plumes. The hot patch (Dubuffet et al., 2000b) beneath the surface displayed previously in Fig. 5a, corresponding to a low conductivity layer, shows a distinctly higher radiative conductivity than the lattice conductivity. This is caused by a rather high temperature at this shallow depth. For the model with $R = 5$ and $f = 8$, the ratio $k_{rad}/k_{lat}$ shows greater variations than the model with $R = 5$ and $f = 1$. This ratio ranges from 0.3 to 14.3 for the model with $f = 8$, whereas it ranges from 0.03 to 1.5 for the model with $f = 1$. The lattice conductivity is smaller than the radiative conductivity only in the upper part of the top boundary layer. The radiative conductivity is greater than the lattice conductivity elsewhere. The greatest values of the ratio lie in the hot patch beneath the top boundary layer, where the radiative conductivity is more than 10 times greater than the lattice conductivity. The stabilization of the flow results from an enhancement in the radiative conductivity of the boundary layers. For this value of $f = 8$, the radiative conductivity is everywhere greater than the lattice conductivity, in particular within the bottom boundary layer.

In order to demonstrate the stabilizing effects on the flow from a purely depth-dependent conductivity, we have conducted one experiment with a thermal conductivity in which we have removed both the radiative component and the temperature-dependence of the lattice conductivity. Other types of depth-dependent thermal conductivities, based on a seismic equation of state, have been proposed by Anderson (1987) and were used in numerical modelling (Yuen and Zhang, 1989; Leitch et al., 1991; Tackley, 1996a). The purely depth-dependent thermal conductivity has the following expression:

$$k_2(z) = k_0 \left(1 + \rho g \frac{K' z}{K}\right) \tag{7}$$

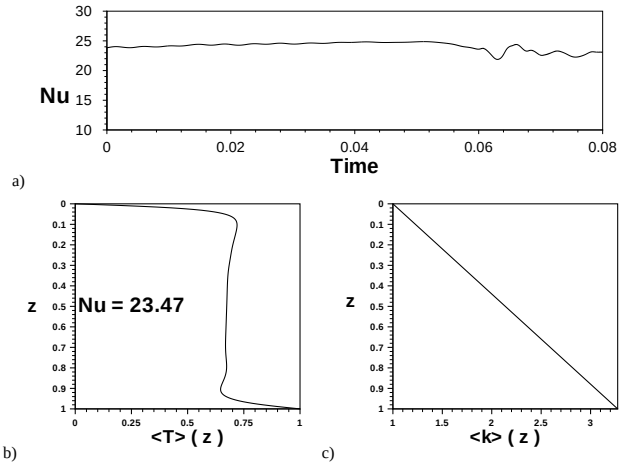


**Fig. 11.** Evolution with time of the surface Nusselt number **(a)**, horizontally temperature profile $\langle T \rangle(z)$ **(b)**, and the horizontally averaged conductivity profiles $\langle k_{rad} \rangle$ (dashed-dotted line), $\langle k_{lat} \rangle$ (dashed line) and $\langle k \rangle$ (solid line) **(c)**, for the model with the expression for thermal conductivity $k(z) = k_{lat}(z)$ (Eq. 7), $Ra = 10^6$ and $R = 0$.

The thermal conductivity increases only with depth. We note that the non-linear term with $(\nabla T)^2$ is now no longer present in the right hand side of the temperature Eq. (4). Figure 10 shows the results for a convective model with the expression of the conductivity given by Eq. (7), $Ra = 10^6$ and $R = 0$. The flow (Fig. 10a) is more stable than in the case with the expression of the reference variable conductivity (Hofmeister, 1999) with $f = 1$ (Fig. 1). The flow consists of 3 large cells plus a smaller one. Some instabilities are present in the thermal boundary layers. The stabilization of the flow results from the large increase in depth of the conductivity (Fig. 10c). We show that the increase in the conductivity with depth does exert a stabilizing effect on the global flow. Figure 11 show the associated evolution of the surface Nusselt number, $\langle T \rangle$ and $\langle k \rangle$ profiles. We see that without the decreasing influence of $k_{lat}(T)$ the conductivity increases by a factor of 3 across the mantle, as in the conductivity model based on seismic velocities by Anderson (1987).

The influence of internal heating on the purely depth-dependent thermal conductivity is shown in Fig. 12, where the temperature and stream function fields in addition to the thermal conductivity field are displayed. The time-dependence is stronger with internal heating, as evidenced by the growing complexity of the plume structures, and the cell sizes have increased. The larger aspect-ratio flow causes a reduction in the surface Nusselt number to 19.4 (Fig. 13b). Other panels of Fig. 13 include the time-history of the surface Nusselt number, the horizontally averaged temperature $\langle T \rangle$, which has increased because of the internal heating, and the conductivity $\langle k \rangle$ profile.

The lattice conductivity ($k_{lat}$) is both temperature- and depth-dependent. We have studied the effects on the flow, of the depth-dependence and the temperature-dependence of the lattice conductivity. First, we have removed the tempera-

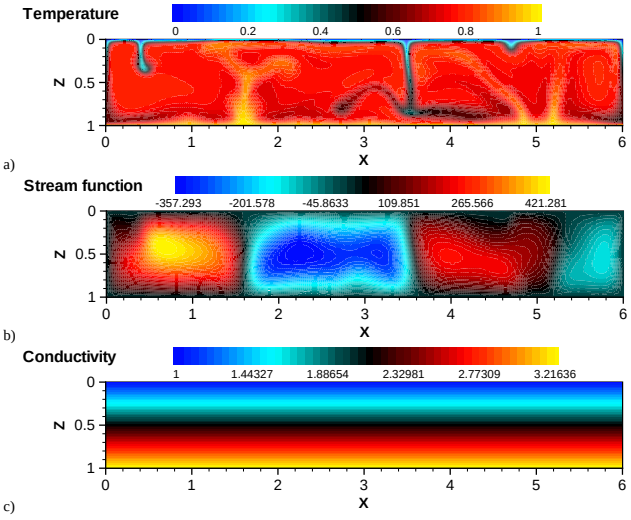


**Fig. 12.** Temperature field **(a)**, stream function **(b)**, and the thermal conductivity field **(c)**, for the model with the expression for thermal conductivity $k(z) = k_{lat}(z)$ (Eq. 7), $Ra = 10^6$ and $R = 5$.

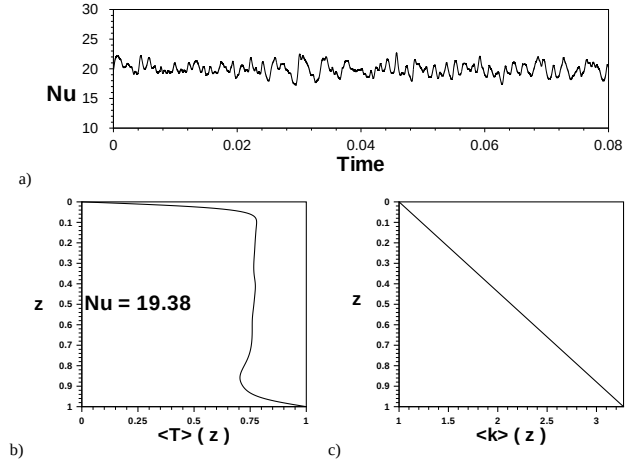


**Fig. 13.** Evolution with time of the surface Nusselt number **(a)**, horizontally averaged temperature $\langle T \rangle(z)$ **(b)**, and the horizontally averaged conductivity profiles $\langle k_{rad} \rangle$ (dashed-dotted line), $\langle k_{lat} \rangle$ (dashed line) and $\langle k \rangle$ (solid line) **(c)**, for the model with the expression for thermal conductivity $k(z) = k_{lat}(z)$ (Eq. 7), $Ra = 10^6$ and $R = 5$.

ture dependence form the lattice conductivity. We have used in our convective model, the following expression for $k_{lat}(z)$:

$$k_{lat}(z) = k_0 \left(1 + \rho g \frac{K' z}{K}\right) \tag{8}$$

This is the same as Eq. (7) used in Figs. 12 and 13. The expression of the thermal conductivity becomes now:

$$k_3(T, z) = f \times k_{rad}(T) + k_{lat}(z) \tag{9}$$

We note that $\partial k_3 / \partial T$ is positive now. Figure 14 shows the results for a model with the expression of the thermal conductivity given by Eq. (9), $f = 1$, $Ra = 10^6$ and $R = 5$.

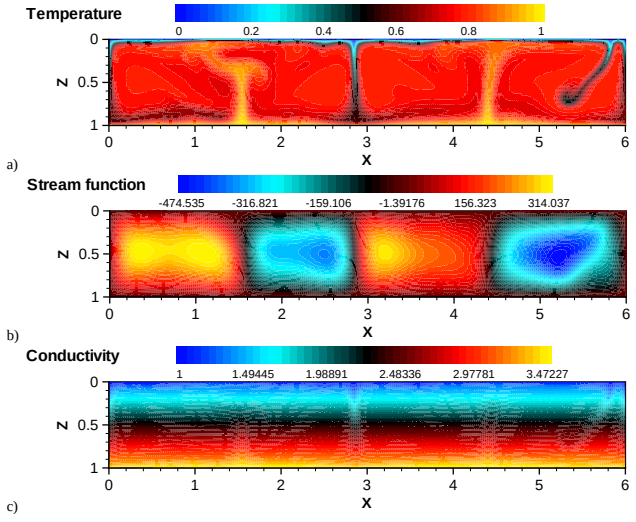


**Fig. 14.** Temperature field **(a)**, stream function **(b)**, and the thermal conductivity field **(c)**, for the model with the expression for $k_3(T, z)$ given by Eq. 8 and Eq. 9, $f = 1$, $Ra = 10^6$ and $R = 5$.

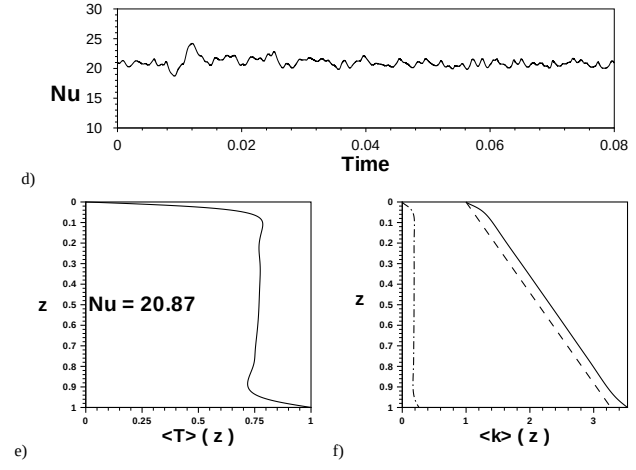


**Fig. 15.** Evolution with time of the surface Nusselt number **(a)**, horizontally averaged temperature profile $\langle T \rangle(z)$ **(b)**, and the horizontally averaged conductivity profiles $\langle k_{rad} \rangle$ (dashed-dotted line), $\langle k_{lat} \rangle$ (dashed line) and $\langle k \rangle$ (solid line) **(c)**, for the model with the expression for $k_3(T, z)$ given by Eq. 8 and Eq. 9, $f = 1$, $Ra = 10^6$ and $R = 5$.

The flow with $k_3(T, z)$ is now much stable than in the model with the same values of the parameters ($f = 1$, $Ra = 10^6$ and $R = 5$) and the inclusion of the temperature-dependent lattice conductivity (Fig. 5). Some small instabilities persist in the thermal boundary layers (Fig. 14a). The flow consists of 4 cells (Fig. 14b). The conductivity field (Fig. 14c) shows larger variations of the conductivity than in the case with the temperature-dependence of $k_{lat}$ (Fig. 5c). The mantle conductivity is always greater than the surface conductivity. This results in the stabilization of the global flow, much more so than the case with $k_2(z)$ in Fig. 12. The lateral variations of the conductivity are quite not visible at the bottom.

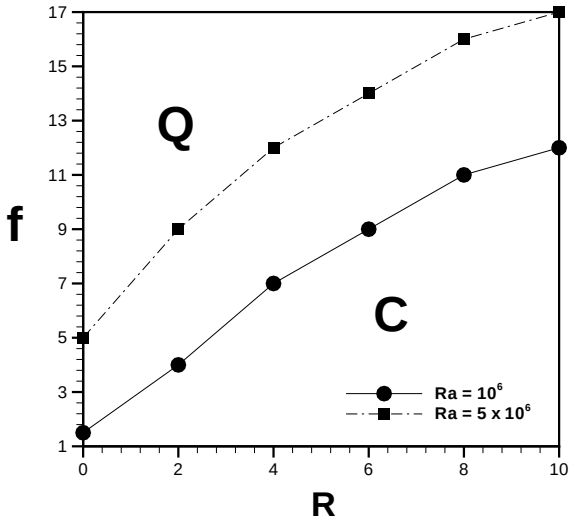


**Fig. 16.** Domain diagram delineating the chaotic ($C$) and the quasi-steady ($Q$) regimes. The weight factor $f$ is the ordinate and the dimensionless internal heating rate $R$ is the abscissa. The critical $f_c$ values are marked by points, with the upper set representing $Ra = 5 \times 10^6$, and the lower set $Ra = 10^6$. Values of $f_c$ are determined up to $f_c + 0.5$ for $10^6$ and $f_c + 2$ for $Ra = 5 \times 10^6$. We note that the solutions more than $f_c + 2$ are locked on to a steady-state solution with hardly any signs of time-dependence.

This results from a sharp increase in the lattice conductivity with depth. This combination of both radiative and depth-dependent thermal conductivity results in the greatest stabilization of all flows examined up to now, since the destabilizing influence of the lattice conductivity has now been removed. In Fig. 15 we show the associated evolution of the surface Nusselt number, the horizontally averaged temperature and the profiles for the $\langle k_{rad} \rangle$, $\langle k_{lat} \rangle$ and $\langle k \rangle$. With a higher temperature at the CMB, like 4000 K, $\langle k_{rad} \rangle$ can approach values close to 1, the surface value of the conductivity.

We have carried out a series of time-dependent calculation using a high resolution of $1025 \times 257$ points for locating the locus of points separating the chaotic ($C$) regime and the quasi-steady ($Q$) regime. Each run has been integrated for 30 000 timesteps to insure that we have gone beyond the transient regime. Several runs are needed for each point displayed in Fig. 16, where we have constructed a domain diagram delineating the values of $f_c$ for different values of internal heating from $R = 0$ to $R = 10$. Thus this undertaking is quite computationally intensive. Values of $f_c$ are determined up to 2 units in $f$ for the higher $Ra$. Hence a non-trivial amount of computational resources is required for constructing Fig. 16. Larger values of $f_c$ are needed to stabilize the flow with an increasing amount of internal heating (larger $R$) and increasing convective vigor (larger $Ra$). Number of upwellings increases with both $Ra$ and $R$ for the solutions displayed in Fig. 16. An increase in $f$ leads to fewer upwellings. Let us remark here that flows with values of $f$ in excess of $f_c + 2$ are rendered to be steady states. The trend for $f_c$

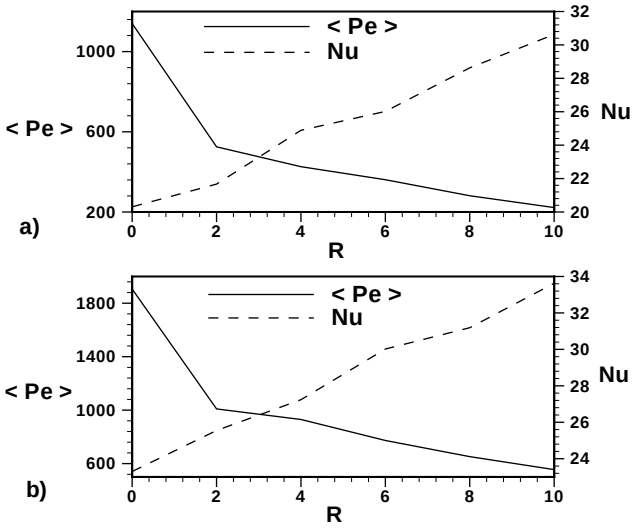


**Fig. 17.** Volumetrically averaged value of the local Peclet number ($\langle Pe \rangle$), and the horizontally averaged surface Nusselt number ($Nu$), as a function of the dimensionless internal heating ($R$), for models with $Ra = 10^6$ **(a)**, and $Ra = 5 \times 10^6$ **(b)**. All values displayed in this figure are given by the models displayed in Fig. 16, which gives the values of $f_c$ for each case. These values have been averaged over the last 200 time steps. The local Péclet number is calculated at each grid point by the square root of the velocity components.

displays an asymptotic character with increasing $R$. It tends toward around 14 for $Ra = 10^6$ and 20 for $Ra = 5 \times 10^6$. The values of $f_c$ increase somewhat with a larger $Ra$, but the relative gain in $f_c$ is smaller than the increase in $Ra$.

We show in Fig. 17 that these stabilizing phenomena are operating in a regime very far from a weakly convective regime. In this figure we plot as a function of $R$ for the points shown in Fig. 16 the corresponding volumetrically averaged value of the local Péclet number ,$\langle Pe \rangle$, and the horizontally averaged surface Nusselt number, $Nu$. These values, with $\langle Pe \rangle$, between 200 and 2000, and $Nu$ greater than 20, demonstrate overwhelmingly that the nonlinear control wielded by variable thermal conductivity still lingers on in spite of the presence of strong convective motions. Inspection of Fig. 17 shows the somewhat paradoxical trend that with greater radiative participation due to higher $f$ values, smaller values of $\langle Pe \rangle$ are produced with increasing $R$ but also greater heat transport, as evidenced by the higher values of $Nu$ with larger values of $R$. This same phenomenon was also found in the steady-state calculations (van den Berg et al., 2001) for a radiatively dominated thermal conductivity model, in which the largest $Nu$ was found for a given $Ra$. But these parameter values for radiative conductivity fall outside the geophysically relevant range.

The results shown in Figs. 16 and 17 support the previous findings of Dubuffet et al. (2000a) that the influence of variable thermal conductivity is very much still present in the high Rayleigh number regime, contrary to the conventional conjecture that diffusion effects can only operate effectively in the weakly nonlinear convective regime.

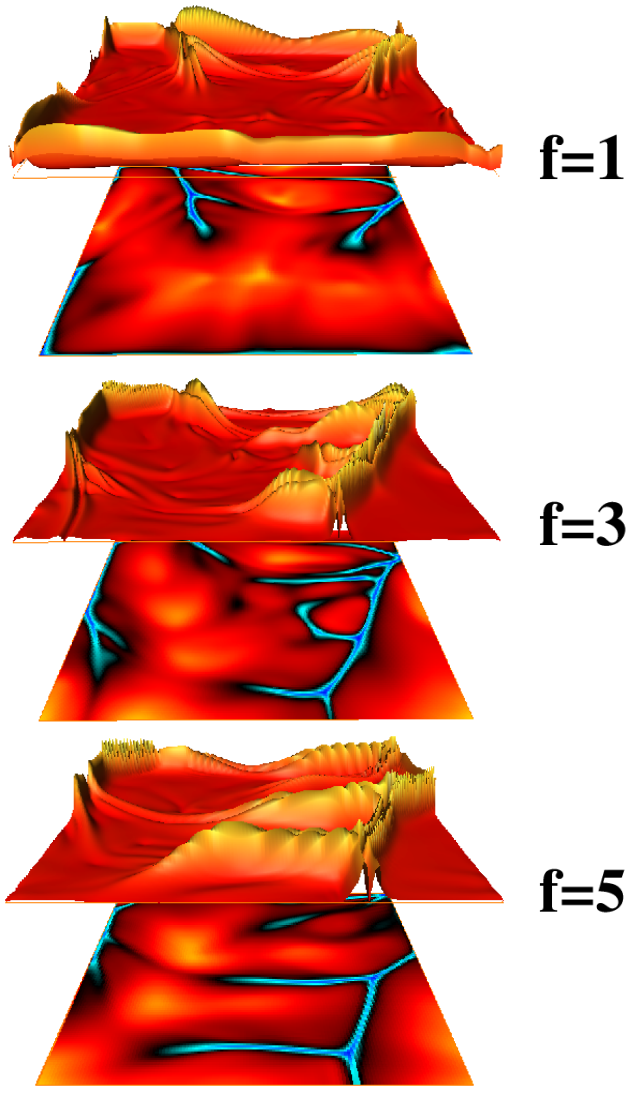


**Fig. 18.** $L_2 - norm$ of the horizontal gradient of the temperature (top surface) on the entire plane located under the top surface at a depth of $z = 0.05$, and the temperature field (bottom surface) in the same plane, for a 3-D model of convection with a Rayleigh number of $Ra = 5 \times 10^6$, a dimensionless internal heating rate of $R = 0$, and three different values of the weight factor $f$, 1, 3 and 5. $257 \times 257 \times 257$ grid points are used in a box with dimensions of $4 \times 4 \times 1$.

The effects of increasing $f$ on stabilizing planforms are also observed in 3-D configurations. This phenomenon is illustrated in Fig. 18, where we have shown that the stabilization of the platforms also takes place with increasing value of $f$. Three values of $f$ ranging from 1, 3, and 5 have been considered for $Ra = 5 \times 10^6$ and $R = 0$ in an aspect-ratio $4 \times 4 \times 1$ box. We have shown both the $L_2 - norm$ of the horizontal gradient of the temperature superimposed upon the surface temperature field. With the increase of $f$ much sharper $\nabla T$ gradients are developed along with the formation of coherent horizontal platforms as manifested by formation of the narrow boundary-layer structure on the sur-

face. This pattern is similar to those found in Soret-driven convection with nonlinear diffusion coefficient (Cerbino et al., 2002), whose mass diffusivity derivative with respect to the composition has the same positive sign as $dk_{rad}/dT$. We suggest that the stability of the 3-D planform against chaotic fluctuations is caused by the nonlinear focusing due to the temperature-dependence of the radiative thermal conductivity.

## 4 Discussion

In this work we have employed a current model of mantle thermal conductivity which has some very interesting nonlinear properties in the temperature. We have focussed here on constant viscosity because variable viscosity would cause other nonlinear feedback processes between the momentum and energy equations. Contrary to traditional thinking, we have found that the influence of the nonlinear diffusive nature of the temperature equation extends out to the convection regime with relatively high Péclet number or high Rayleigh number. These far-reaching effects of temperature-dependent conductivity on mantle convection have already been demonstrated by Dubuffet et al. (2000a) for Rayleigh numbers as high as $7 \times 10^6$ in a Cartesian 3-D geometry, where the sinking cold currents with higher conductivity were found to be assimilated thermally much more readily than those with a constant conductivity. We can explain this somewhat counter-intuitive behaviour on the basis of a nonlinear interaction between the boundary type flow with a huge contribution in $\nabla T$ and the variable conductivity, which provides a feedback for sustaining the pervasive influence of nonlinear conductivity at high Rayleigh number. A similar kind of feedback has also been found in the nonlinear diffusion equation in two-phase flow within a geothermal context (Woods, 1999).

We have demonstrated that there is a sharp transition, similar to a phase change, in the time-dependent behaviour with $f$, which delineates the relative importance between the radiative and the lattice components of the conductivity. This critical value $f_c$ is very close to the reference value $f = 1$ present in Hofmeister's model (Hofmeister, 1999) for purely basally-heated configuration and does not change much with higher Rayleigh number. However, with the inclusion of mantle internal heating of even half of the chondritic value, the value of $f_c$ increases by a factor of nearly an order in magnitude, thus illustrating another feedback effect arising between internal heating, and temperature-dependent conductivity (van den Berg et al., 2002). This notion of the stabilizing influence of radiative thermal conductivity was first discovered by the time-dependent simulations by Matyska et al. (1994), who employed a purely radiative thermal conductivity, with the exactly same formulation as used by Mac Donald (1959). We have also lent support to this idea of the ability of radiative conductivity to suppress time-dependent flows in the lower mantle by carrying out two separate numerical experiments in which the nonlinear temperature dependent components of the conductivity are switched off in a systematic manner, leaving finally a linear thermal conductivity with only depth-dependence. Therefore, the radiative component of thermal conductivity now joins the ranks of other mantle properties, such as depth-dependent thermal expansivity (Hansen et al., 1993), depth-dependent viscosity (Hansen et al., 1993; Zhang and Yuen 1995; Bunge et al., 1996; Dubuffet et al., 2000c; Forte and Mitrovica, 2001), and endothermic phase transition (Tackley, 1996b), which are all mechanisms responsible for inducing mantle flow to a less chaotic environment with fewer plumes and longer horizontal wavelengths . This tendency is caused by the formation of strong thermal attractors in the solution space, whose physical manifestations are the recurrent plume-plume merging events (Vincent and Yuen, 1988) occurring at nearly the same place in the bottom boundary layer. The value of $f_c$ will undoubtedly be lowered by depth-dependent thermal expansivity, as the thermal buoyancy is reduced locally in the bottom boundary layer. We have furthermore demonstrated that this stabilization effect from radiative thermal conductivity also works in 3-D, similar to the effects played by nonlinear diffusion coefficient in colloidal convection (Cerbino et al., 2002). Higher temperatures for the deep mantle than the value assumed here with a temperature of 3000K at the core-mantle boundary would cause $f_c$ to be lower, because of the greater stabilizing influence of $k_{rad}(T)$ at higher temperatures.

What are then the geophysical implications of this work? Our results would suggest that in order to have relatively stationary deep mantle plumes with variable thermal conductivity, the lower mantle should contain very little radioactive heating (Anderson, 1979) for a reference conductivity model (Hofmeister, 1999) with $f = 1$. For internal heating of the amount proposed by Kellogg et al. (1999) for the deep lower mantle, which was two times the chondritic value ($R$ around 25), there would be a very strong agitation of the mantle flow. However, enhanced thermal conductivity from a D′′ layer with a high temperature at the CMB, enriched by iron infiltration from the outer core (Manga and Jeanloz, 1996), would indeed help to stabilize the deep mantle plumes and may influence the number of plumes in both the upper and lower mantle (Malamud and Turcotte, 1999). Mixing of geochemical anomalies in the deep mantle would also be influenced by the relative contribution of radiative component in the conductivity, since the intrinsic time-dependence of mantle convection and the number of hotspots are linked to the particular value of $f_c$, which depends on many factors, such as the amount of radioactive heating, the temperature at the core-mantle boundary, the depth-dependent properties of the lower mantle.

*Acknowledgements.* We would like to thank A. M. Hofmeister, A. P. van den Berg, R. Cerbino, M. Giglio, D. L. Turcotte, S. Karato and M. Monnereau for stimulating discussions. We thank the enlightening reviews by the two conscientious reviewers. This research has been supported by the geophysics section of the National Science Foundation and the Complex Fluids program of the Dept. of Energy.

## References


Anderson, D. L.: Chemical stratification of the mantle, J. Geophys. Res. 84, 6297–6298, 1979.

Anderson, D. L.: A seismic equation of state II, Shear properties and thermodynamics of the lower mantle, Phys. Earth Planet. Int., 45, 307–323, 1987.

Bunge, H.-P., Richards, M. A., and Baumgardner, J. R.: Effect of depth-dependent viscosity on the planform of mantle convection, Nature, 379, 436–438, 1996.

Cerbino, R., Valiati, A., and Giglio, M.: Observation of a rapid-onset Soret-driven instability at very high Rayleigh number, submitted to Phys. Rev. Lett., 2002.

Dubuffet, F., Yuen, D. A., and Rabinowicz, M.: Effects of a realistic mantle thermal conductivity on the patterns of 3-D convection, Earth Planet. Sci. Lett., 171, 401–409, 1999.

Dubuffet, F. and Yuen, D. A.: A thick pipe-like heat-transfer mechanism in the mantle: nonlinear coupling between 3-D convection and variable thermal conductivity, Geophys. Res. Lett., 27, 1, 17–20, 2000.

Dubuffet, F., Yuen, D. A., and Yanagawa, T.: Feedback effects of variable thermal conductivity on the cold downwellings in high Rayleigh number convection, Geophys. Res. Lett., 27, 18, 2981–2984, 2000a.

Dubuffet, F., Yanagawa, T. K., and Yuen, D. A.: Persistently hot coherent structures in the shallow upper mantle: Manifestations of temperature-dependent thermal conductivity, Fall Meeting abstract, American Geophysical Union, 2000b, http://www.agu.org/.

Dubuffet, F., Rabinowicz, M., and Monnereau, M.: Multiple-scales in mantle convection, Earth Planet. Sci. Lett., 178, 351–366, 2000c.

Christensen, U. R.: Instability of a hot boundary layer and initiation of thermo-chemical plumes, Ann. Geophysicae, 2, 311–320, 1984.

Forte, A. M. and Mitrovica, J. X.: Deep-mantle high-viscosity flow and thermochemical structure inferred from seismic and geodynamic data, Nature, 410, 1049–1056, 2001.

Hansen, U. and Ebel, A.: Time-dependent thermal convection - a possible explanation for a multi-scale flow in the Earth's mantle, Geophys. J., 94, 181–191, 1988.

Hansen, U., Yuen, D. A., Kroening S. E., and Larsen, T. B.: Dynamical consequences of depth-dependent thermal expansivity and viscosity on mantle circulations and thermal structure, Phys. Earth. Planet. Inter., 77, 205–223, 1993.

Hofmeister, A. M.: Mantle values of thermal conductivity and the geotherm from phonon lifetimes, Science, 283, 1699–1706, 1999.

Hofmeister, A. M.: Thermal conductivity of spinels and olivines from vibrational spectroscopy: Ambient conditions, American Mineralogist, 86, 1188–1208, 2001.

Kardar, M., Parisi, G., and Zhang, Y.-C.: Dynamic scaling of growing interfaces, Phys. Rev. Lett., 56, 889–892, 1986.

Kellogg, L. H., Hager, B. H., and van der Hilst, R. D.: Compositional stratification in the deep mantle, Science, 283, 1881–1884, 1999.

Kim, M., Bertram, M., and Pollmann, M., et al.: Controlling chemical turbulence by global delayed feedback: pattern formation in catalytic CO oxidation on Pt(110), Science, 292, 1357–1360, 2001.

Larsen, T. B. and Yuen, D. A.: Ultrafast upwelling bursting through the upper mantle, Earth Planet. Sci. Lett., 146, 393–400, 1997.

Leitch, A. M. and Yuen, D. A.: Internal heating and thermal constraints on the mantle, Geophys. Res. Lett., 16, 1407–1410, 1989.

Leitch, A. M., Yuen, D. A., and Sewell, G.: Mantle convection with internal-heating and pressure-dependent thermal expansivity, Earth Planet. Sci. Lett., 102, 213–232, 1991.

Mac Donald, G. J. F.: Calculations on the thermal history of the Earth, J. Geophys. Res., 64, 1967–2000, 1959.

Malamud, B. D. and Turcotte, D. L.: How many plumes are there?, Earth Planet. Sci. Lett., 174, 113–124, 1999.

Malevsky, A. V., Yuen, D. A., and Weyer, L. M.: Viscosity and thermal fields associated with strongly chaotic non-Newtonian thermal convection, Geophys. Rev. Lett., 19, 27–30, 1992.

Manga, M. and Jeanloz, R.: Implications of a metal-bearing chemical boundary layer in D′′ for mantle dynamics, Geophys. Res. Lett., 23, 22, 3091–3094, 1996.

Matyska, C., Moser, J., and Yuen, D. A.: The potential influence of radiative heat transfer on the formation of megaplumes in the lower mantle, Earth Planet. Sci. Lett., 125, 255–266, 1994.

McKenzie, D. P., Roberts, J. M., and Weiss, N. O.: Convection in the Earth's mantle: toward a numerical simulation, J. Fluid Mech., 62, 465–538, 1974.

Monnereau, M. and Quéré, S.: Spherical shell models of mantle convection with tectonic plates, Earth Planet. Sci. Lett., 184, 575–587, 2001.

Morton, K. W. and Mayers, D. F.: Numerical Methods of Partial Differential Equations, Chapter 3, Cambridge University Press, 1994.

Ogawa, M., Schubert, G., and Zebib, A.: Numerical simulations of three-dimensional thermal convection in a fluid with strongly temperature-dependent viscosity, J. Fluid Mech., 233, 299–328, 1991.

Olson, P. L., Schubert, G., Anderson, C., and Goldman, P.: Plume formation and lithosphere erosion: A comparison of laboratory and numerical experiments, J. Geophys. Res., 93, 15 065–15 084, 1988.

Ott, E., Sauer, T., and Yorke, J.: Coping with Chaos: Analysis of Chaotic Data and the Exploitation of Chaotic Systems, J. C. Wiley Inc., New York, 1994.

Pelletier, J. D.: Self-organization and scaling relationships of evolving river networks, J. Geophys. Res., 104, B4, 7359–7375, 1999.

Richter, F. M., Nataf, H. C., and Daly, S. F.: Heat transfer and horizontally averaged temperature of convection with large viscosity variations, J. Fluid Mech., 129, 173–192, 1983.

Siegel, R. and Howell, J. R.: Thermal Radiation Heat Transfer, Mc Graw-Hill, New York, 1972.

Solomatov, V. S. and Moresi, L. N.: Time-dependent stagnant lid convection on the Earth and other terrestrial planets, J. Geophys. Res., 105, B9, 21 795–21 818, 2000.

Tackley, P. J.: Effects of strongly variable viscosity on three-dimensional compressible convection in planetary mantles, J. Geophys. Res., 101, 3311–3332, 1996a.

Tackley, P. J.: On the ability of phase transitions and viscosity layering to induce long wavelength heterogeneity in the mantle, Geophys. Res. Lett., 23, 15, 1985–1988, 1996b.

Thompson, P. F. and Tackley, P. J.: Generation of mega-plumes from the core-mantle boundary in a compressible mantle with temperature-dependent viscosity, Geophys. Res. Lett., 25, 1999–2002, 1998.

Tozer, D.: Heat transfer and convection currents, Phil. Trans. Roy. Soc. London, A258, 252–271, 1965.

Tozer, D. C.: The present thermal state of the terrestrial planets, Phys. Earth Planet. Inter., 6, 182–197, 1972.

van den Berg, A. P., Yuen, D. A., and Steinbach, V.: The effects of variable thermal conductivity on mantle heat transfer, Geophys. Res. Lett., 28, 5, 575–578, 2001.

van den Berg, A. P., Yuen, D. A., and Allwardt, J. R.: Feedback effects from variable thermal conductivity and mantle internal heating: Implications for massive melting and secular cooling of the mantle, Phys. Earth Planet. Inter., 129, 359–375, 2002.

Vincent, A. P. and Yuen, D. A.: Thermal attractor in chaotic convection with high Prandtl number fluids, Phys. Rev. A., 38, 328–334, 1988.

Vincent, A. P. and Yuen, D. A.: Transition to turbulent thermal convection beyond $Ra = 10^{10}$ detected in numerical simulations, Phys. Rev. E, 61, 5, 5241–5247, 2000.

Woods, A. W.: Liquid and vapor flow in superheated rock, Annu. Rev. Fluid Mech., 31, 171–200, 1999.

Yuen, D. A. and Schubert, G.: Mantle plumes: a boundary layer approach for Newtonian and non-Newtonian temperature-dependent rheologies, J. Geophys. Res., 81, 2499–2510, 1976.

Yuen, D. A. and Zhang, S.: Equation of state and rheology in deep mantle convection, in: Perovskites, (Eds) Navrotsky, A. and Weidner, D. J., American Geophysical Union, Washington D. C., AGU Monograph, 45, 131–146, 1989.

Zhang, S. and Yuen, D. A.: The influences of lower-mantle viscosity stratification on 3-D spherical-shell mantle convection, Earth Planet. Sci. Lett., 132, 157–166, 1995.

Zerr, A., Diegeler, A., and Boehler, R.: Solidus of the Earth's deep mantle, Science, 281, 243–246, 1998.

Ziman, J. M.: Electrons and Phonons: The Theory of Transport Phenomena in Solids, Clarendon Press, Oxford, pp. 550, 1962.